Assessing the Efficiency of Sodium Ferrate Production by Solution Plasma Process

Sina Samimi-Sedeh, Ehsan Saebnoori, Amirreza Talaiekhozani, Mohamad Ali Fulazzaky, Martin Roestamy & Ali Mohammad Amani

Plasma Chemistry and Plasma Processing

ISSN 0272-4324
Volume 39
Number 4

Plasma Chem Plasma Process (2019)
39:769-786
DOI 10.1007/s11090-019-09989-2

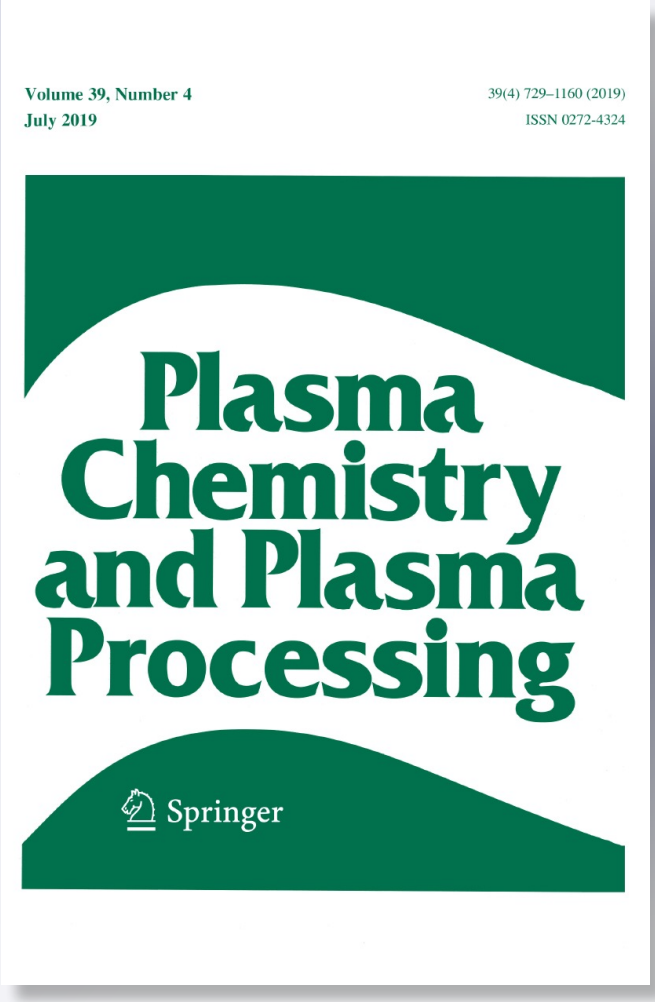

Springer

Plasma Chemistry and Plasma Processing (2019) 39:769–786
https://doi.org/10.1007/s11090-019-09989-2

ORIGINAL PAPER

Assessing the Efficiency of Sodium Ferrate Production by Solution Plasma Process

Sina Samimi-Sedeh[1] · Ehsan Saebnoori[1] · Amirreza Talaiekhozani[2] · Mohamad Ali Fulazzaky[3] · Martin Roestamy[3] · Ali Mohammad Amani[4]

Received: 1 January 2019 / Accepted: 4 April 2019 / Published online: 15 April 2019

Abstract

Application of sodium ferrate (Na_2FeO_4) is considered as the environmental friendly and cost-effective method for oxidation, coagulation and disinfection processes of water and wastewater treatment. Even though many methods of Na_2FeO_4 production have been proposed, they are still a challenge for the production of large Na_2FeO_4 quantity. This study aims to verify the optimum operating conditions of Na_2FeO_4 production by solution plasma process (SPP) of using both anode and cathode made of low-carbon steel placed in electrolyte solution with a distance of 3 cm. The results showed that the efficiency of Na_2FeO_4 production by SPP that does not obey Faraday's law is higher than that by conventional electrochemical process. The optimum operating conditions of SPP were verified in 16 M NaOH solution at 30 °C and imposed by 35 V of the voltage while the maximum concentration and the average particle size of the Na_2FeO_4 production as high as 14.7 mM and 35 nm, respectively, were verified. The maximum current efficiency of 512% and the minimum energy consumption of 6 kWh/kg were verified for the formation of Na_2FeO_4 during 2 h due to an increased activity of OH^- ions. A new approach of large Na_2FeO_4 production has been proposed to support the development of advanced technologies in water and wastewater treatment.

Keywords Current efficiency · Energy consumption · Environmental friendly method · Electrolyte solution · Optimum operating condition

Electronic supplementary material The online version of this article (https://doi.org/10.1007/s11090-019-09989-2) contains supplementary material, which is available to authorized users.

✉ Mohamad Ali Fulazzaky
fulazzaky@unida.ac.id

[1] Advanced Materials Research Center, Department of Materials Engineering, Islamic Azad University, Najafabad Branch, Daneshgah Blvd, Najafabad, Iran

[2] Department of Civil Engineering, Jami Institute of Technology, Isfahan, Iran

[3] School of Postgraduate Studies, Djuanda University, Jalan Tol Ciawi No. 1, Ciawi, Bogor 16720, Indonesia

[4] Department of Medical Nanotechnology, Shiraz University of Medical Sciences, Shiraz, Iran

Introduction

The demands for water and wastewater treatment industry continuously increase due to the increasing of population, economic and industrial growth from the year to year. More than 20 methods with its own advantages and disadvantages have been proposed for the treatments of water and wastewater. Many types of oxidizing agents, coagulants and disinfectants can be used in the processes of water and wastewater treatment [1, 2]. The use of ferric sulfate ($Fe_2(SO_4)_3$), aluminum sulfate ($Al(SO_4)_3$) and ferric chloride ($FeCl_3$) is useful for coagulant agents [3]. The use of chlorine (Cl_2), sodium hypochlorite (NaClO), chlorine dioxide (ClO_2) and ozone (O_3) is useful for oxidizing agents and disinfectants [4]. It is very common for the treatments of water and wastewater to use the oxidants and disinfectants such as ferrate(VI), chlorine, ozone and hydrogen peroxide. The chlorine is widely used to treat the surface water and groundwater for drinking water production in many developing countries because of its low operating cost and high removal efficiency. However, the chlorine disinfection was not able to destroy some species of such as anthrax and cryptosporidium [5, 6]. In addition, chlorine can react with organic compounds to form undesirable byproducts like trihalomethanes in the treated water [7–9]. The cost of water and wastewater treatment by ozonation process could be relatively high in the capital and operating costs. Since ozone is unstable and reactive, it has a very short retention time under normal conditions and is dependent on the environmental conditions like temperature, pH and mineral content [10]. Therefore, the application of sodium ferrate (Na_2FeO_4), or ferrate(VI) particles, has been recommended as an environmentally friendly method for the treatment of water and wastewater because of they have the properties of high oxidation potential, effective disinfection ability and selective formation of the nontoxic byproduct [9]. The disinfection process of using the Na_2FeO_4 particles can generate a byproduct of $Fe(OH)_3$, which causes the coagulation and flocculation for use in the removal of colloidal particles [11, 12]. The ferrate(VI) compounds can be found in the form of different salts such as Na_2FeO_4, K_2FeO_4, Ba_2FeO_4, and Ag_2FeO_4. The particles of ferrate(VI) have the morphology of appearing smoother and more granular when comparing with the morphology of the particles resulting from ferric iron [13]. A natural organic matter can be transformed into more hydrophilic compounds by ferrate(VI) oxidation while the produced hydrophilic compounds have a low affinity with colloids and are less adsorbed on colloids to produce a less negative surface charge [14]. The electrochemical synthesis of ferrate(VI) can be carried out an in situ Na_2FeO_4 formation by the anodic dissolution of a carbon steel wire in concentrated NaOH solution. Therefore, the recent development of advanced wastewater treatment has been recaptured an interest on ferrate(VI) as an emerging wastewater treatment agent [15].

Three major methods can be proposed to produce the Na_2FeO_4 particles, such that: (1) dry oxidation of iron at high temperature by heating or melting the iron oxides in the presence of oxygen in an environment with high alkalinity, (2) wet oxidation of iron using the chemical oxidizing agents by oxidation of trivalent iron salt at high alkalinity and in the presence of chlorine or hypochlorite and (3) electrochemical process of using iron or its alloys as the anode electrode and an electrolyte solution of NaOH or KOH [16, 17]. The formation of Na_2FeO_4 can be electrochemically described by an anodic reaction of $Fe + 8\ OH^- \rightarrow FeO_4^{2-} + 4\ H_2O + 6\ e^-$ and by a cathodic reaction of $2\ H_2O + 2\ e^- \rightarrow H_2 + 2\ OH^-$ [18]. In spite of the different compositions of iron oxide sheath occur at the temperature range of 300–800 °C, any carbon steel wire treated above 600 °C may lose its wire-like shape because of the void coalescence as a result

of the shrinkage and collapse effects [19]. The increased oxidation rate for the oxidation of iron in dry and wet O_2 at 500 and 600 °C can cause a smaller grain size in the hematite layer and leads to faster movement of iron ions [20]. The production of Na_2FeO_4 particles by electrochemical process is more common than other methods because it does not require any chemical agent [21, 22]. One of the major problems in conventional electrochemical process of decreasing efficiency after continuous process for making ferrates is due to the passivation of electrode surface [11, 23, 24], which is not suitable for the industrial scale production of Na_2FeO_4 particles [25, 26].

The use of high voltage to create sparks on the anode surface has been attracting attentions at the research community since 2005. The contact glow discharge electrolysis (CGDE) can be used for the electrochemical process of being characterized by high-voltage electrochemical capacitor to create plasma at electrode–electrolyte interface [27]. The CGDE process has been widely used in the synthesis of nanoparticles and named as the solution plasma process (SPP) [28–30]. Solution plasma can have the advantages of such as simplicity of process, no need of gas supply, continuous improvement capability [31], easy mass production and controllable particle size [32]. In the case of CGDE process, the plasma generates at the cathode/solution interface. Since the electrical resistance heating of the electrolyte solution may concentrate at the cathode/solution interface, the heat of electrolyte solution near the cathode can reach at a boiling point to generate a gas layer containing of hydrogen gas and steam. Once gas layer has been generated at the cathode surface, the current cannot increase anymore but decreases due the cathode and the electrolyte solution are not touching each other to current boundary at breakdown point. It is suggested that gas layer can form glow discharge plasma when the voltage is sufficiently high. A glow discharge with the light emission may occur at a certain voltage. The intensity of light emission increases with increasing of the voltage, which means that the net area of discharge expanded with increasing of the voltage. The discharge could be a partial-plasma and the transition to full-plasma can occur at certain voltage without any edge shielding. A current can jump temporarily and then maintains a steady value. In contrast, the transition to full-plasma would be suppressed by edge shielding where the average current can reach at a certain value even if SPP uses the same voltage, and the average electrolyte solution temperature decreases slightly [30]. Electrochemical formation of Na_2FeO_4 particles normally obeys the Faraday's law with its high efficiency in an optimal condition [33]. However, SPP as the abnormal electrochemical process that does not follow the Faraday's law can have the different optimum conditions for the electrochemical generation of Na_2FeO_4 particles [34–36]. Efficiency of SPP is always higher than that of theoretical calculation because of the free energy of radical ions (such as H_2O_2, OH^-, H^+, e^- and HO_2^-) is high [37]. Therefore, the production of Na_2FeO_4 particles by SPP is expected to be more efficiency than conventional electrochemical process.

In spite of many researches have been driven by the ideas of putting the application of Na_2FeO_4 into practice [1, 2, 9, 11], optimizing the efficiency and rate of the Na_2FeO_4 synthesis could be a big obstacle in future development of ferrates electrochemical synthesis due to the passivation of the electrode can lead to a decrease in the efficiency of Na_2FeO_4 production [38]. The objectives of this study are: (1) to produce the large amount of Na_2FeO_4 particles by SPP with alternating current (AC) and (2) to evaluate the effects of voltage, NaOH concentration and initial temperature on the behaviors of Na_2FeO_4 production.

Materials and Methods

Materials

This study used the carbon steel wire of 2-mm diameter as anode. Upper part of the anodic electrode was shielded by quartz-glass tube to obtain an exposed length of 10 mm. The exposed part of anodic electrode can be functioned as the net actual electrode. A steel circle sheet with its thicknesses of 1-mm and its surface area of 75×50 mm^2 was used as cathode. The cathode was bent in the form of circle around the anode. The anode was placed at center of the electrolyte solution with a distance of 3 cm from the cathode and 4 cm away from the bottom of electrolyte solution bath. The cathode was kept in the electrolyte solution by a quartz rod. All materials and chemical compounds of the analytical grades were purchased from Merck, Tehran, Iran. Table 1 shows the chemical composition of cathode and anode.

Experimental Procedure

Due to the available energy of AC source used by SPP with a frequency of 50 Hz sinusoidal voltage and voltage varying from 20 to 55 V to initiate the spark under atmospheric pressure and room temperature can suddenly increase the temperature of electrolyte solution, the initial temperature must be controlled using the water bath of being operated at 4 °C and placed around the electrochemical cell to reach below 45 °C. The electrolyte solution of 500 mL was homogenized using the magnetic stirrer at speed of 350 rpm. The temperature of water bath was homogenized using the mechanical stirrer at speed of 248 rpm. The oxide layers from the surface of anode were removed using 400, 600, 800, and 1200 grit SiC abrasive papers. The electrochemical cell was cleaned with acetone and dried and then isolated from the atmospheric environment. Potentiodynamic polarization curves of the iron electrode in different NaOH concentrations were measured using a conventional standard three-electrode electrochemical test system. This work used the pure platinum foil as counter electrode and the saturated calomel electrode (SCE) as reference. After an initial delay of 60 min, the potential electrolyte was verified to increase at a scan rate of 1 mV/s, starting from 250 mV below the open circuit potential. All corrosion testing was repeated three times with nearly identical results.

Effects of voltage (20–55 V), NaOH concentration (8–18 M) and temperature (5–45 °C) on the formation of Na_2FeO_4 particles by SPP were analyzed during 5 min of the experiment. Effect of voltage on the Na_2FeO_4 production was investigated by keeping the NaOH concentration at 16 M and temperature at 25 °C of the solution constant. Effect of NaOH concentration on the Na_2FeO_4 formation was investigated by keeping the voltage at 35 V and temperature at 25 °C of the solution constant. Effect

Table 1 Composition of the anode and cathode

Electrode	Chemical composition (%)										
	Ni	Cr	S	P	Mn	Si	C	Mo	Al	Co	Fe
Cathode	7.30	19.3	0.01	0.028	1.18	0.29	0.06	0.1	0.01	0.201	Balance
Anode	0.005	0.025	0.014	0.022	0.187	0.045	0.047	0.013	0.022	0.002	Balance

of temperature on the production of Na_2FeO_4 particles was investigated by keeping the constant voltage of 35 V and the constant NaOH concentration of 16 M. Particle size and chemical composition were investigated using the transmission electron microscope (TEM) analysis (Philips CM120) and the X-ray diffractometry (XRD) analysis (Philips PW3040), respectively, after obtaining the optimum operating conditions of Na_2FeO_4 production. Additionally, the current efficiency and energy consumption by SPP were investigated by using the laboratory power supply (ED-345BM) to create the atmospheric pressure plasma in the electrolyte solution. The efficiency and concentration of the Na_2FeO_4 particles were analyzed using the Optizen 3220UV Double Beam UV–Vis Spectrophotometer. Because of the maximum absorption of Na_2FeO_4 occurred at a wavelength of 505 nm, the calculation of Na_2FeO_4 concentration was entirely carried out based on the absorbance at the wavelength of 505 nm. A calibration curve helps determine the concentration of unknown electrolyte solution by converting the raw absorbance data to molar concentration when it is placed on the curve. The corrosion rate of carbon steel wire was measured using the PARSTAT 2273 Potentiostat (Princeton Applied Research) in various NaOH concentrations of the electrolyte solution.

Data Calculation

One of the important factors in the production of Na_2FeO_4 is the amount of energy consumption. The total energy consumption can be calculated using the equation [34] of:

$$E = \frac{VIt}{m} \tag{1}$$

where E is the energy consumption (in W h/kg), V is the applied voltage (in V), I is the electric current (in A), t is the time of conducting the experiment (h), and m is the mass of Na_2FeO_4 particles (kg).

The purity of Na_2FeO_4 particles can be calculated using the Beer–Lambert equation [39] of:

$$P = \frac{A}{\varepsilon} \times 0.1 \times \frac{M}{W} \times 100\% \tag{2}$$

with

$$A = \varepsilon LC \tag{3}$$

where P is the purity of Na_2FeO_4 particles (in %), A is the value of absorbance (dimensionless), ε is the attenuation coefficient (in mol^{-1}), which is obtained from the calibration curve and then calculated using Eq. (3). M is the molecular mass of Na_2FeO_4 (in g mol^{-1}), W is the weight of sample (in g), L is the width of quartz cuvette (in cm), and C is the concentration of Na_2FeO_4 (in mol L^{-1} or M). The fact that when the electrolyte solution was placed in a quartz square tube with an inner width of 1 cm, A/ε ratio is the Na_2FeO_4 concentration in electrolyte solution.

Using Eq. (2) permits us to calculate the purity of Na_2FeO_4 particles. The proper production of Na_2FeO_4 particles can be obtained by mixing the Na_2FeO_4 powder in 100 mL of the saturated NaOH solution and stirred at 400 rpm at 10 °C for 5 min. Then the Na_2FeO_4 concentration in NaOH solution was analyzed using the UV–Vis spectrophotometry. In this work, the crystal size of Na_2FeO_4 can be investigated using the TEM analysis.

Results and Discussion

Effects of Voltage, NaOH Concentration, and Temperature on the Na_2FeO_4 Production

Effect of Voltage on Na_2FeO_4 Production

The results (Table 2) show the effect of voltage ranged from 20 to 55 V on the Na_2FeO_4 production when the NaOH concentration in solution was fixed at 16 M for the experiment imposed using an average current source of 7.3 A at 25 °C during 5 min. It is recognized that spark ignition delay time is the delay time of ignition energy delivery as spark to beginning of the steady flame propagation [40]. An increase in the voltage from 20 to 55 V can lead to abruptly fall the spark ignition delay time to first second and increases the final electrolyte solution temperature from 16 to 45 °C. Therefore, the formation of plasma occurs sooner, attributing it to more electrical potential energy. The maximum Na_2FeO_4 concentration of 14.3 mM was obtained at 35 V of the voltage. The SPP imposed by a voltage of 20 V was not able to vaporize the surrounding liquid and to produce the plasma in center of the gas layer around the ferrous anode. The first spark confirms the initiation of plasma around the anode after 164 s of the delay time when the voltage increases up to 30 V. Table 2 shows that the formation of Na_2FeO_4 at 30 V is five times higher than that at 20 V of the voltage. The evidence of high quantity of Na_2FeO_4 particles attributes to the formation of plasma occurred by imposing 30 V of the voltage. By increasing the voltage from 20 to 30 V, a surface melting occurs even if there is no initial spark. This may lead to overheating and excessive generation of high-energy particles such as H_2O_2. When the voltage is greater than 35 V, a degeneration of plasma may occur and leads to the reduction of Na_2FeO_4 concentration in electrolyte solution. The production of Na_2FeO_4 by conventional electrochemical process can increase the density of current to reach higher than its critical value, depending on electrolyte concentration, anode, cathode and temperature. The increasing of reaction rate can lead to an evolution of oxygen at the anode surface [41] and the reduction of hydrogen at the cathode surface [34, 35, 42]. The reduction of hydrogen at cathode surface may decrease the efficiency of current density and the rate of Na_2FeO_4 production. However, an increase of the current density can cause the decomposition of Na_2FeO_4 compounds at high temperature [43].

This study verified that an increase in the voltage from 35 to 55 V this can lead to increasing of the final electrolyte solution temperature from 34 to 45 °C and the

Table 2 Effect of voltage on the Na_2FeO_4 production in 16 M NaOH solution at 25 °C for 5 min

Voltage (V)	Average current (A)	Spark ignition delay time (s)	Final solution temperature (°C)	Na_2FeO_4 concentration (mM)
20	7.3	–	16	1.9
30	7.3	164	32	10.1
35	7.3	39	34	14.3
40	7.3	21	38	13.2
45	7.3	4	44	11.7
55	7.3	First second	45	7.9

temperature gradually decreases from the electrode rod towards the wall of electrolytic cell. An increase of the final electrolyte solution temperature could be due to the generated heat surrounding anode cannot be balanced with a cooling capacity of the electrolytic cell. The average current of around 7.3 A reflects essentially no change during the SPP experiment, as shown in Fig. 1. The temperature of 68 °C was verified at around the anode from which the plasma sparks, decreased to 62 °C at the electrolytic cell interface and then decreased to 45 °C at outside of the electrolytic cell when a voltage of 55 V was imposed on the electrode. The decreasing of temperature from 68 °C at around the anode to 49 °C at the electrolytic cell interface and then to 34 °C at outside of the electrolytic cell was verified when the electrode was imposed by a voltage of 35 V. The thermodynamic of high temperature in electrolyte solution can cause to a sudden decomposition of Fe(VI) to Fe(III) and to Fe(II). The formation of Na_2FeO_4 suggested based a product and pathway consistent with the observed colored electrolyte solution can be described by the chemical equation of: $2\ H^+ + H_2O_2 + 2\ Fe(II) \rightarrow 2\ Fe(III) + 2\ H_2O$ and then by the chemical equation of: $2\ Na^+ + 2\ OH^- + Fe(III) + 2\ (H^+ + \bullet O_2^-) \rightarrow 2\ H_2O + Na_2FeO_4 + 3\ e^-$ [44]. The decomposition of Na_2FeO_4 can accelerate when the additional iron ions are added to the electrolyte solution [36]. The production of high-energy particles and free radical of H_2O_2 in electrolyte solution increases with increasing of the imposed voltage [45, 46]. The efficiency of Na_2FeO_4 production may improve when the H_2O_2 concentration increases but to not higher that its optimum concentration in electrolyte solution of containing certain NaOH concentration. The results (Fig. 2a) of verifying the effect of voltage variation on the color property of Na_2FeO_4 particles observed in 16 M NaOH solution at 25 °C during 5 min of the experiment show that an increase in the imposition of voltage from 35 to 55 V can cause the color of Na_2FeO_4 particles to gradually change from reddish purple to a white there is due to the increasing of energy imposed to move electrons from one orbital to another.

The weight loss of anode was measured at various voltages after 5 min of conducting the experiment. The results (Fig. 2b) show that the weight loss of anode increased from 0.073 to 0.770 g with increasing of the voltage from 20 to 35 V could be due to the electrode consumption by electrolyte solution can have the optimum operating voltage of 35 V. Then, an increase in the voltage from 35 to 55 V this can lead to a decrease in the weight loss of 0.200 g from 0.770 to 0.570 g because of any voltage spike higher than 35 V would be consumed by other reactions of Na_2FeO_4 decomposition rather than electrode consumption. The integral value of current is zero and this may not be able to estimate the distribution of potential and protective current density at anodic or cathodic

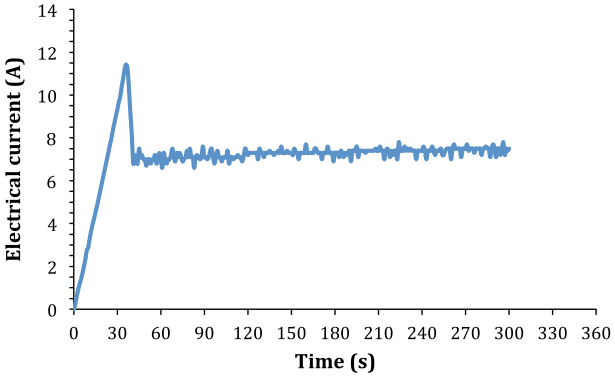

Fig. 1 A plot of electrical current versus time of the experiment imposed with a voltage of 20 V and 16 M NaOH concentration in electrolyte solution

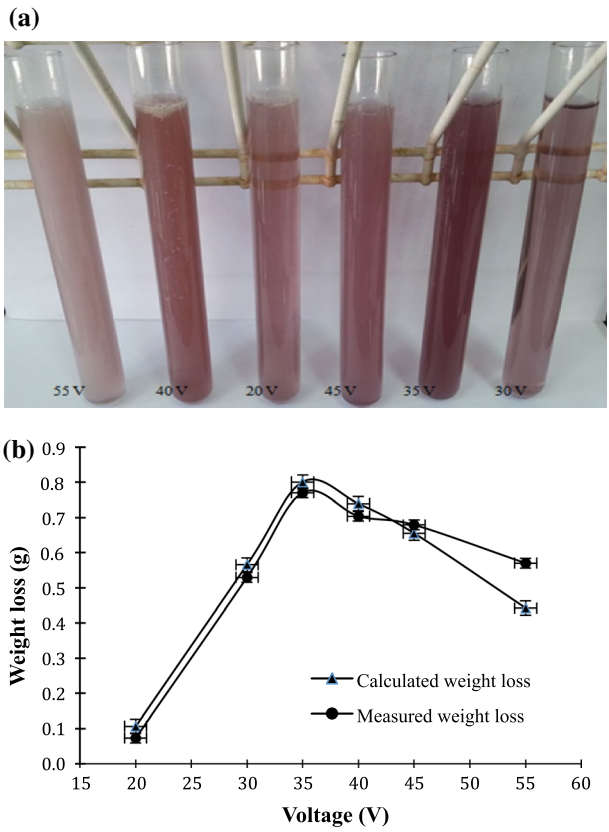

Fig. 2 Effect of voltage on **a** the color of Na_2FeO_4 particles and **b** the weight loss of Na_2FeO_4 particles for the experiment by solution plasma process in 16 M NaOH electrolyte solution at 25 °C during 5 min (Color figure online)

part of the voltage circuits. Therefore, it cannot be explained which part of the current has been used for the formation of Na_2FeO_4 particles or oxygen evolution [47]. The same is true for hydrogen evolution in parallel with the reduction of Na_2FeO_4 compounds. Because of the ratio between two electric currents used for an individual electrode reaction changes with changing of the voltage, it is not possible to determine the exact portion of electric current used for each electrochemical reaction in spite of the change in Na_2FeO_4 synthesis efficiency can be attributed to either the portion of anodic or cathodic reaction at different voltages.

The rate of electrode weight loss can be calculated since the quantity of Na_2FeO_4 production has been verified. Noted that (1) the measured weight loss is the different weight of electrode before and after the experiment of SPP and (2) the calculated weigh loss is the Na_2FeO_4 concentration in electrolyte solution measured using the UV–Vis spectroscopy. Figure 2b shows that the calculated weight loss of approximately 0.030 g higher than the measured weight loss was verified when the amplitude of voltage signal imposed on the monitored electrodes was 40 V. However, the measured weight losses of 0.024 and 0.128 g higher than the calculated weight losses were verified when the amplitudes of voltage were imposed at 45 and 55 V, respectively. This means that the kinetics of Na_2FeO_4 decomposition at high voltage is unpredictable. It was not necessary to calculate the purity of Na_2FeO_4 particles using the Beer-Lambert equation due to the A/ε ratio is the Na_2FeO_4 concentration in electrolyte solution.

Effect of NaOH Concentration on Na_2FeO_4 Production

The corrosion tests were performed to get better understanding on the effect of NaOH concentrations on the rate of electrode weight loss. An increase in the electrode weight loss can lead to an increased Na_2FeO_4 formation in the electrolyte solution. Tafel slope noted in term of β is the level of increasing the overpotential to increase the reaction rate by a factor ten and determines the magnitude of the change in the activation energy [48]. A technique of calculating the corrosion rate from electrochemical data does not give any information on the localized corrosion. The rate of corrosion is the speed at which electrode (iron) deteriorates in electrolyte solution. In this work, the unit of corrosion rate is expressed in Mils per year (mpy). The results (Table 3) of verifying the electrochemical corrosion parameters show that the highest corrosion rate of 19.39 mpy was verified for the experiments conducted in 16 M NaOH solution at 25 °C and imposed by 35 V of the voltage during 5 min. The corrosion current density decreases with increasing of the NaOH concentration from 16 to 18 M as the corrosion rate decreases from 19.39 to 14.49 mpy there is because of a high concentration of 18 M NaOH in the electrolyte solution can lower the water activity [49]. An increase in the NaOH concentration from 8 to 18 M can be the only way to decrease the electrical conductivity [22] because of the initiation of spark in electrolyte solution of low NaOH concentration has been occurred earlier at 35 V. An increase in the NaOH concentration from 12 to 18 M in electrolyte solution can significantly increase the rate of the reaction to get verified with increasing of the β_a value from 57 to 140 mV/decade. Two mechanisms of reaction have been proposed for the formation of Na_2FeO_4 particles by electrochemical method, such that: (1) the surface of anode oxidizes to form the oxide layer and then the oxide layer converts to the Na_2FeO_4 formation [50] and (2) the ferrous ions and the iron oxide particles of different valences (intermediate particles) emit into a strongly alkaline electrolyte, which causes the particles converts to the Na_2FeO_4 formation [51]. In case of the formation of Na_2FeO_4 particles by SPP is due to the formation of spark and plasma on the surface of electrodes in electrolyte solution and then the oxidation of them by in situ generation of Na_2FeO_4 in aqueous alkaline solution. The conversion of suspended particles produced by SPP to Na_2FeO_4 depends on the oxidizing capacity of OH^- ions, H_2O_2, and temperature.

The results (Fig. 3a) of Tafel polarization curve tested for different NaOH concentrations at 25 °C show that the current density of 16 M NaOH solution is higher than that of 14 M NaOH solution and then is higher than that of 18 M NaOH solution. It is well matched with the results (Table 3) of verifying the corrosion rate that the corrosion rate of 19.39 mpy is higher than that of 14.77 mpy and then is higher than that of 14.49 mpy for the NaOH concentrations of 16, 14, and 18 M in electrolyte solution, respectively.

Table 3 Effect of NaOH on the corrosion rate observed at 25 °C and 35 V for 5 min

NaOH concentration (M)	β_a (mV/decade)	β_c (mV/decade)	Corrosion current density (μA cm^{-2})	Potential (mV)	Corrosion rate (mpy)
8	56	− 25	8.9	− 863	8.19
12	57	− 49	12.2	− 959	11.21
14	140	− 46	16.1	− 1079	14.77
16	131	− 49	21.2	− 1099	19.39
18	111	− 49	15.8	− 1055	14.49

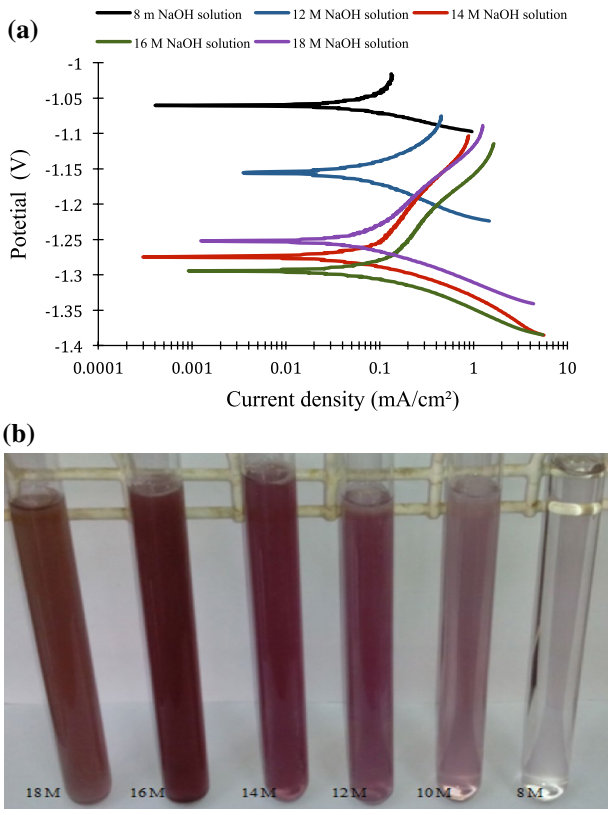

Fig. 3 Effect of NaOH concentration on the formation of Na_2FeO_4 particles for the experiment of solution plasma process imposed by 35 V of the AC source at 25 °C during 5 min; with **a** the tafel polarization curves of low-carbon steel and **b** the color change of Na_2FeO_4 production (Color figure online)

The rate of corrosion affected by free H_2O molecules and accelerated by OH^- is due to the OH^- ions increase with increasing of the NaOH concentration. The rate of corrosion tends to increase with an increase in the velocity of motion of the electrolyte solution over the surface of electrode. The modification of the electrode surface can enhance the corrosion resistance [52]. The velocity of free H_2O molecules movement reduces when the 18 M NaOH concentration of apparently imposed electrolyte solution. This study verified that the optimum operating condition of Na_2FeO_4 production was occurred in 16 M NaOH solution.

The results (Table 4) of UV–Vis spectroscopy show that the formation of Na_2FeO_4 particles increases from 3.9 to 14.3 mM with increasing of the NaOH concentration from 8 to 16 M. A low Na_2FeO_4 production of 3.9 mM could be due to the synthesized Na_2FeO_4 particles may rapidly decompose if the large amount of free H_2O molecules in 8 M NaOH solution exists. However, the mobilization of free H_2O molecules significantly decreases when the NaOH concentration reaches up to 18 M and this may affect a decrease of the corrosion rate yielding the reduction of Na_2FeO_4 formation, there is due to the decomposition of Na_2FeO_4 particles is low [41] and the balance of dissolved Fe(II), Fe(III) and Fe(VI) species is stable [22, 53, 54]. The increasing of Na_2FeO_4 particles in electrolyte solution was verified by gradually increasing the color density from white in 8 M to brown in 18 M NaOH solution, as shown in Fig. 3b.

Table 4 Effect of NaOH on the Na_2FeO_4 production at 25 °C and 35 V for 5 min

NaOH concentration (M)	Ignition time (s)	Final solution temperature (°C)	Na_2FeO_4 concentration (mM)
8	First second	43	3.9
10	First second	41	4.3
12	21	38	9.0
14	29	35	12.1
16	39	34	14.3
18	–	30	3.1

Effect of Temperature on Na_2FeO_4 Production

The results (Table 5) of UV–Vis spectroscopy show that the maximum Na_2FeO_4 concentration of 14.7 mM was verified in 16 M NaOH solution with the initial temperature of 30 °C. The atmospheric pressure plasma could be not initiated at an initial temperature of 5 °C for the experiment of 5 min. The plasma can initiate to start the sparks during the first few seconds inside the electrolyte solution with the temperature range of 35–45 °C and this leads to an increase in the temperature from 37 to 42 °C at outer wall of the electrolytic cell. An increase in the temperature can increase the conductivity of electrolyte solution to early starting the initiation of spark up until the formation of Na_2FeO_4 particles [36, 55]. When the initial temperature of electrolyte solution was set at 45 °C, the final temperature of 68 °C was verified at around the anode in the spark region, decreased to 59 °C at the electrolytic cell interface and then decreased to 45 °C at outside of the electrolytic cell for the experiment in 16 M NaOH solution imposed by 35 V of the voltage during 5 min. However, the decreasing of final temperature from 68 °C at around the anode to 51 °C at the electrolytic cell interface and then to 36 °C at outside of the electrolytic cell was verified when the initial temperature of electrolyte solution was set at 30 °C. An increase in the temperature of electrolyte solution can increase the activity of OH^- ions and leads to increase the Na_2FeO_4 production efficiency. However, the high stability of Na_2FeO_4 synthesis is obviously due to the low temperature of SPP. The efficiency of Na_2FeO_4 production may decrease after 2 h of the experiment when the temperature of SPP is higher than 35 °C [35]. Degradation of passive film on the anode can occur at high temperature due to the activity of OH^- ions increases and prevents a rapid drop of the Na_2FeO_4 production efficiency. The degeneration of Na_2FeO_4 particles is very fast when the temperature of SPP is higher than 70 °C.

Table 5 Effect of temperature on Na_2FeO_4 production in 16 M NaOH solution at 35 V for 5 min

Initial solution temperature (°C)	Ignition time (s)	Final solution temperature (°C)	Na_2FeO_4 concentration (mM)
5	–	25	1.5
15	186	30	7.9
25	39	34	14.3
30	15	36	14.7
35	5	39	11.4
45	First second	45	5.8

This study suggested according to the plot of anode weight loss versus temperature (see Fig. 4) that the production rate of Na_2FeO_4 particles around the anode increases with increasing of the initial temperature of electrolyte solution. Figure 4 shows that an increase in the anode weight loss of 0.719 g from 0.072 to 0.789 g with increasing of the initial temperature from 5 to 30 °C is due to the dissolution of anode increases. However, the increasing of temperature to higher than 30 °C this may lead to a decrease of the anode weight loss due to part of the electrons moving from cathode to anode are consumed by other reactions of Na_2FeO_4 decomposition in electrolyte solution rather than anode dissolution. The true rate of electrochemical reactions is amplified by more electrons consumed around the cathode compared to around the anode for the production of Na_2FeO_4 particles. The plots (Fig. 4) of the measured and calculated anode weight loss versus temperature show that the calculated anode weight loss is 0.024 g higher than the measured anode weight loss at an initial electrolyte solution temperature of 30 °C to reveal the optimum operating temperature of producing Na_2FeO_4 particles. However, the measured anode weight losses of 0.648 and 0.434 g are 0.010 and 0.109 g higher than the calculated anode weight losses of 0.638 and 0.325 g for the electrolyte solution with its initial temperatures of 35 and 45 °C, respectively, due to the decomposition of Na_2FeO_4 particles increases with increasing of the electrolyte solution temperature after reaching higher than 30 °C during 5 min of the experiment.

Investigation of Na_2FeO_4 Production at Optimum Operating Conditions

The production of Na_2FeO_4 particles under the optimum operating conditions of using 16 M NaOH solution, imposing by 35 V and running at 30 °C must be investigated for understanding the efficiency of Na_2FeO_4 production and energy consumption, the size distribution and surface morphology, as well as the XRD plasma phase analysis of Na_2FeO_4 formation.

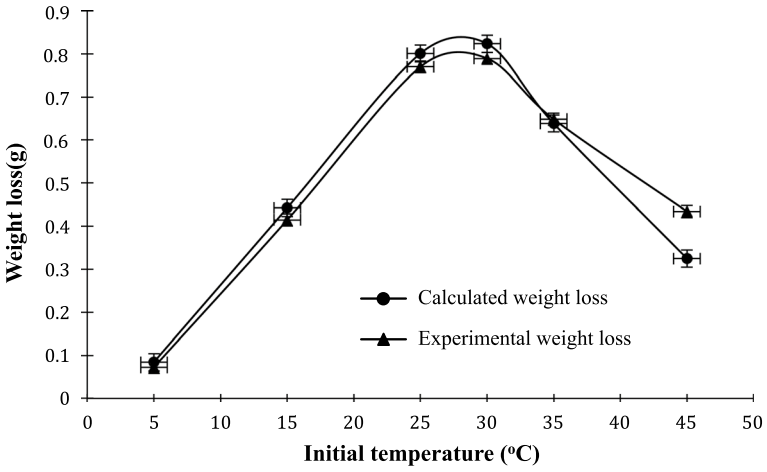

Fig. 4 Effect of initial temperature on the anode weight loss in 16 M NaOH solution for the experiment of solution plasma process imposed by a voltage of 35 V during 5 min

Efficiency of Na_2FeO_4 Production and Energy Consumption

Once the plasma is initiated, it is possible to accelerate the particles in electrolyte solution for producing the OH^- and e^- elements of much higher energy to participate in the formation of Na_2FeO_4 particles [34, 41, 56]. Even though the rate of Na_2FeO_4 formation increases with increasing of the temperature, the stability of Na_2FeO_4 in electrolyte solution occurs at low temperature [35]. It is difficult to set the experimental conditions with high temperature near the anode and low temperature at a certain distance beyond the anode aperture due to the electrolyte solution flows, except the in situ arrangement by the mechanism of plasma formation [57–59]. A high temperature of the anode can increase the activity of OH^- ions and leads to increase the rate of Na_2FeO_4 formation. This study verified that the current efficiency of SPP to produce Na_2FeO_4 reaches seven times higher than that of conventional electrochemical process. The plots (Fig. 5) of energy consumption and current efficiency of the Na_2FeO_4 production versus time show that an optimum operating condition with a current efficiency range of 501–512% reaches when the time of experiment is at a range of 2–3 h. The other processes of Na_2FeO_4 production verified that the electrode becomes passive after a while and the efficiency of Na_2FeO_4 production decreases [23, 43, 60]. The productions of Na_2FeO_4 particles as high as 1.76 and 8.64 g were verified for the energy consumptions of 11 kWh/kg during 0.5 h and 9 kWh/kg during 2 h of the experiment, respectively, with the Na_2FeO_4 purity of 98.9%. When there is no passivation occurred in plasma solution this can be affected by high voltage, synthesis and reaction mechanism of the Na_2FeO_4 formation, and viscosity reduction mechanism. The energy consumption begins to increase from 6 kWh/kg at 3 h to 12 kWh/kg at 8 h of the experiment, as can be seen in Fig. 5.

Size Distribution and Surface Morphology

The TEM image of Na_2FeO_4 particles reveals the microstructure that the average particle size of approximately 35 nm being characterized with its size distribution in the range of 10–90 nm was verified from nine TEM images (see Fig. S1 of Supplementary material) like the one shown in Fig. 6. The synthesis of nanocrystalline and monodispersed Na_2FeO_4 particles of the uniform spherical shape was observed under given optimum operating conditions of SPP. Spherical, ellipsoidal and elongated hematite particles can be obtained in

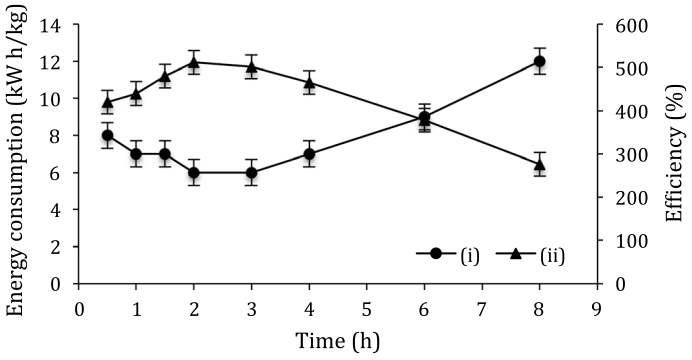

Fig. 5 Effect of time on (i) the energy consumption and (ii) the current efficiency of the Na_2FeO_4 production in 16 M NaOH solution at 30 °C

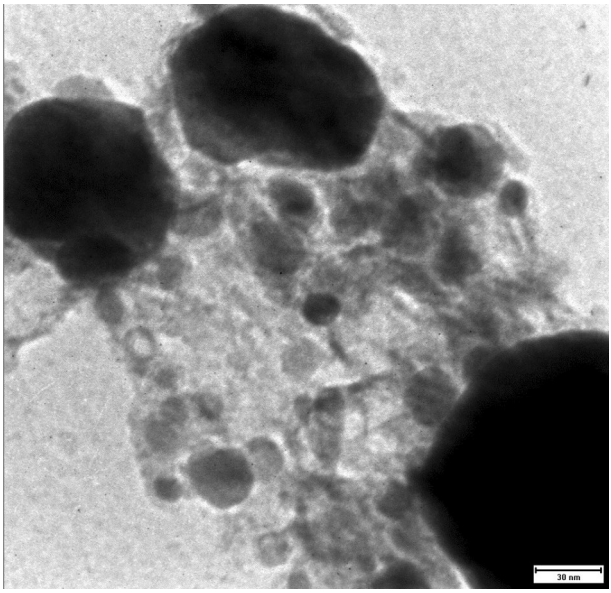

Fig. 6 TEM image of Na_2FeO_4 particles observed under given optimum operating conditions of solution plasma process

the presence of ascorbic acid by the reaction of chemical precipitation of $FeCl_3$ and NaOH [61].

XRD Analysis

The results (Fig. 7) of the XRD analysis indicates the existence of Na_2FeO_4 particles with a very high intensity at the 2-theta of 30, following by the 2-theta of 20 and then by the 2-theta of 34. It has been reported that the plasma synthesis of nanoparticles with different

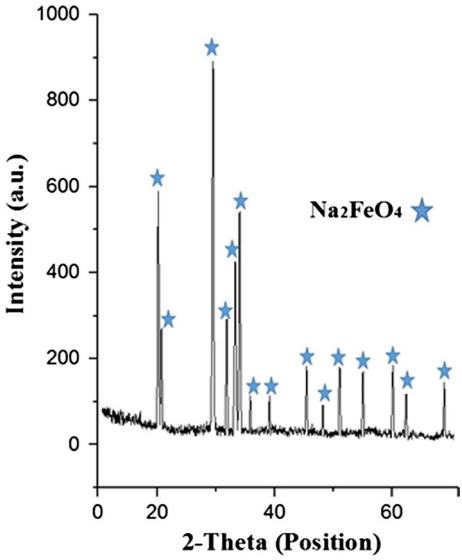

Fig. 7 XRD pattern of Na_2FeO_4 particles

iron oxides occurs when the time of electrolysis and viscosity of the fluid increase [62]. CO_2 from air can be easily absorbed by the electrolytic cell to form Na_2CO_3 [63, 64]. The electrolytic cell must be isolated from the atmospheric environment and kept at stable temperature for the production of Na_2FeO_4 by SPP in the range of pH 9.2-10.

Conclusions

This study aims to understand the formation mechanism of Na_2FeO_4 particles by SPP. The optimum operating conditions of Na_2FeO_4 production in 16 M NaOH solution were obtained when the SPP imposed by 35 V of the voltage at 30 °C of the initial electrolyte solution temperature. The increases of voltage higher than 35 V and initial electrolyte solution temperature higher than 30 °C can lead to an increased decomposition rate of Na_2FeO_4 compounds. A decrease in the NaOH concentration of lower than 16 M in electrolyte solution can cause to shorten the time to start the sparks due to the conductivity of electrolyte solution increases. There is no plasma atmosphere initiated at 35 V with increasing of up to 18 M NaOH concentration because of the conductivity of the electrolytic cell is low. An increase in the current efficiency of up to 512% could be due to the formation of OH^- ions and H_2O_2. A decrease of the current efficiency over time after passing the optimum time could be due to the passivation of the electrode. The efficiency of Na_2FeO_4 production by SPP was verified seven times higher than that of conventional electrochemical process due to the presences of plasma, high-energy particles and different mechanisms of the Na_2FeO_4 formation. A new approach of the large Na_2FeO_4 production has been proposed to contribute to growing improvement of the advanced technologies in water and wastewater treatment.

References

1. Song Y, Men B, Wang D, Ma J (2017) On-line batch production of ferrate with an chemical method and its potential application for greywater recycling with Al(III) salt. J Environ Sci 52:1–7
2. Zhou Z, Fang S, Chen H, Ji J, Wu J (2017) Trials of treating decentralized domestic sewage from a residential area by potassium ferrate(VI). Water Air Soil Pollut 228:316
3. Katsoyiannis IA, Tzollas NM, Tolkou AK, Mitrakas M, Ernst M, Zouboulis AI (2017) Use of novel composite coagulants for arsenic removal from waters—experimental insight for the application of polyferric sulfate (PFS). Sustainability 9:590
4. Banach JL, Sampers I, Van Haute S, van der Fels-Klerx HJ (2015) Effect of disinfectants on preventing the cross-contamination of pathogens in fresh produce washing water. Int J Environ Res Public Health 12:8658–8677
5. Fadavi M, Baboukani AR, Edris H, Salehi M (2018) Study on high-temperature oxidation behaviors of plasma-sprayed TiB_2-Co composite coatings. J Korean Ceram Soc 55:178–184
6. Peiravi M, Mote SR, Mohanty MK, Liu J (2017) Bioelectrochemical treatment of acid mine drainage (AMD) from an abandoned coal mine under aerobic condition. J Hazard Mater 333:329–338
7. Darvish S, Asadikiya M, Hu B, Singh P, Zhong Y (2016) Thermodynamic prediction of the effect of CO_2 to the stability of $(La_{0.8}Sr_{0.2})_{0.98}MnO_{3\pm\delta}$ system. Int J Hydr Energy 41:10239–10248
8. Liu J, Weinholtz L, Zheng L, Peiravi M, Wu Y, Chen D (2017) Removal of PFOA in groundwater by Fe^0 and MnO_2 nanoparticles under visible light. J Environ Sci Health A Toxic/Hazard Subst Environ Eng 52:1048–1054
9. Talaiekhozani A, Salari M, Talaei MR, Bagheri M, Eskandari Z (2016) Formaldehyde removal from wastewater and air by using UV, ferrate(VI) and UV/ferrate(VI). J Environ Manag 184:204–209
10. Phaniendra A, Jestadi DB, Periyasamy L (2015) Free radicals: properties, sources, targets, and their implication in various diseases. Indian J Clin Biochem 30:11–26

11. Petrov VG, Perfiliev YD, Dedushenko SK, Kuchinskaya TS, Kalmykov SN (2016) Radionuclide removal from aqueous solutions using potassium ferrate(VI). J Radioanal Nucl Chem 310:347–352
12. Wang C, Klamerth N, Huang R, Elnakar H, Gamal El-Din M (2016) Oxidation of oil sands process-affected water by potassium ferrate(VI). Environ Sci Technol 50:4238–4247
13. Goodwill JE, Jiang Y, Reckhow DA, Gikonyo J, Tobiason JE (2015) Characterization of particles from ferrate preoxidation. Environ Sci Technol 49:4955–4962
14. Lv D, Zheng L, Zhang H, Deng Y (2018) Coagulation of colloidal particles with ferrate(VI). Environ Sci Water Res Technol 4:701–710
15. Zheng L, Deng Y (2016) Settleability and characteristics of ferrate(VI)-induced particles in advanced wastewater treatment. Water Res 93:172–178
16. Saebnoori E, Navidinejad A, Baboukani AR (2016) Mechanism study and parameter optimization of A356 aluminum alloy electrochemical polishing. In: Proceedings of Iran international aluminum conference (IIAC2016), 11–12 May 2016, Tehran, IR Iran
17. Talaiekhozani A, Talaei MR, Rezania S (2017) An overview on production and application of ferrate(VI) for chemical oxidation, coagulation and disinfection of water and wastewater. J Environ Chem Eng 5:1828–1842
18. Schmidbaur H (2018) The history and the current revival of the oxo chemistry of iron in its highest oxidation states: Fe^{VI}–Fe^{VIII}. J Inorg Gen Chem 644:536–559
19. Krajewski M, Brzozka K, Lin WS, Lin HM, Tokarczyk M, Borysiuk J, Kowalski G, Wasik D (2016) High temperature oxidation of iron–iron oxide core–shell nanowires composed of iron nanoparticles. Phys Chem Chem Phys 18:3900–3909
20. Pujilaksono B, Jonsson T, Halvarsson M, Svensson JE, Johansson LG (2010) Oxidation of iron at 400–600 °C in dry and wet O_2. Corros Sci 52:1560–1569
21. Wei Y-L, Wang Y-S, Liu C-H (2015) Preparation of potassium ferrate from spent steel pickling liquid. Metals 5:1770–1787
22. Schmidbaur H (2018) The history and the current revival of the oxo chemistry of iron in its highest oxidation states: Fe^{VI}–Fe^{VIII}. Z Anorg Allg Chem 644:536–559
23. De Koninck M, Brousse T, Bélanger D (2003) The electrochemical generation of ferrate at pressed iron powder electrodes: effect of various operating parameters. Electrochim Acta 48:1425–1433
24. He W, Wang J, Yang C, Zhang J (2006) The rapid electrochemical preparation of dissolved ferrate(VI): effects of various operating parameters. Electrochim Acta 51:1967–1973
25. Darvish S, Zhong Y, Gopalan S (2017) Thermodynamic stability of $La_{0.6}Sr_{0.4}Co_{0.2}Fe_{0.8}O_{3-\delta}$ in carbon dioxide impurity: a comprehensive experimental and computational assessment. ECS Trans 78:1021–1025
26. Wang CC, He S, Chen K, Rowles MR, Darvish S, Zhong Y, Jiang SP (2017) Effect of SO_2 poisoning on the electrochemical activity of $La_{0.6}Sr_{0.4}Co_{0.2}Fe_{0.8}O_{3-\delta}$ cathodes of solid oxide fuel cells. J Electrochem Soc 164:F514–F524
27. Kareem TA, Kaliani AA (2012) Glow discharge plasma electrolysis for nanoparticles synthesis. Ionics 18:315–327
28. Hyun K, Saito N (2017) The solution plasma process for heteroatom-carbon nanosheets: the role of precursors. Sci Rep 7:3825
29. Pootawang P, Saito N, Lee SY (2013) Discharge time dependence of a solution plasma process for colloidal copper nanoparticle synthesis and particle characteristics. Nanotechnol 24:055604
30. Saito G, Hosokai S, Tsubota M, Akiyama T (2011) Nickel nanoparticles formation from solution plasma using edge-shielded electrode. Plasma Chem Plasma Process 31:719–728
31. Saito G, Hosokai S, Tsubota M, Akiyama T (2012) Influence of solution temperature and surfactants on morphologies of tin oxide produced using a solution plasma technique. Cryst Growth Des 12:2455–2459
32. Saito G, Hosokai S, Tsubota M, Akiyama T (2011) Synthesis of copper/copper oxide nanoparticles by solution plasma. J Appl Phys 110:023302
33. Ding L, Liu T-X, Li X-Z (2014) Removal of CH3SH with in situ generated ferrate(VI) in a wet-scrubbing reactor. J Chem Technol Biotechnol 89:455–461
34. Alsheyab M, Jiang J-Q, Stanford C (2010) Electrochemical generation of ferrate(VI): determination of optimum conditions. Desalination 254:175–178
35. Barışçı S, Ulu F, Sarkka H, Dimoglo A, Sillanpaa M (2014) Electrosynthesis of ferrate(VI) ion using high purity iron electrodes: optimization of influencing parameters on the process and investigating its stability. Int J Electrochem Sci 9:3099–3117
36. Wang H, Liu Y, Zeng F, Song S (2015) Electrochemical synthesis of ferrate(VI) by regular anodic replacement. Int J Electrochem Sci 10:7966–7976

37. Gao J, Ma D, Lu Q, Li Y, Li X, Yang W (2010) Synthesis and characterization of montmorillonite-graft-acrylic acid superabsorbent by using glow-discharge electrolysis plasma. Plasma Chem Plasma Process 30:873–883
38. Le Formal F, Tétreault N, Cornuz M, Moehl T, Grätzel M, Sivula K (2011) Passivating surface states on water splitting hematite photoanodes with alumina overlayers. Chem Sci 2:737–743
39. Hull CC, Crofts NC (1996) Determination of the total attenuation coefficient for six contact lens materials using the Beer–Lambert law. Ophthal Physiol Opt 16:150–157
40. Sivasubramanian H (2018) Effect of ignition delay (ID) on performance, emission and combustion characteristics of 2-methyl furan-unleaded gasoline blends in a MPFI SI engine. Alex Eng J 57:499–507
41. Yu X, Licht S (2008) Advances in electrochemical Fe(VI) synthesis and analysis. J Appl Electrochem 38:731–742
42. Hassannejad H, Moghaddasi M, Saebnoori E, Baboukani AR (2017) Microstructure, deposition mechanism and corrosion behavior of nanostructured cerium oxide conversion coating modified with chitosan on AA2024 aluminum alloy. J Alloys Compd 725:968–975
43. Ding L (2013) Removal of methyl mercaptan from foul gas by in situ production of ferrate(VI) for odour control. Ph.D. Thesis, The Hong Kong Polytechnic University
44. Sharma VK, Chen L, Zboril R (2016) Review on high valent Fe^{VI} (Ferrate): a sustainable green oxidant in organic chemistry and transformation of pharmaceuticals. ACS Sustain Chem Eng 4:18–34
45. Kim SC, Kim SM, Yoon GJ, Nam SW, Lee SY, Kim JW (2014) Gelatin-based sponge with Ag nanoparticles prepared by solution plasma: fabrication, characteristics, and their bactericidal effect. Curr Appl Phys 14:S172–S179
46. Ren J, Yao M, Yang W, Li Y, Gao J (2014) Recent progress in the application of glow-discharge electrolysis plasma. Cent Eur J Chem 12:1213–1221
47. Bouzek K, Lipovská M, Schmidt M, RoušarDeceased I, Wragg AA (1998) Electrochemical production of ferrate(VI) using sinusoidal alternating current superimposed on direct current: grey and white cast iron electrodes. Electrochim Acta 44:547–557 **(This paper is dedicated to the memory of Professor Ivo Roušar)**
48. Fletcher S (2009) Tafel slopes from first principles. J Solid State Electrochem 13:537–549
49. Zou J-Y, Chin D-T (1987) Mechanism of steel corrosion in concentrated NaOH solutions. Electrochim Acta 32:1751–1756
50. Tiwari D, Lee S-M (2011) Ferrate(VI) in the treatment of wastewaters: a new generation green chemical. In: García Einschlag FS (ed) Wastewater—treatment reutilization. INTECH, London, pp 241–276
51. Sun X, Zu K, Liang H, Sun L, Zhang L, Wang C, Sharma VK (2018) Electrochemical synthesis of ferrate(VI) using sponge iron anode and oxidative transformations of antibiotic and pesticide. J Hazard Mater 344:155–1164
52. Fulazzaky MA, Ali N, Samekto H, Ghazali MI (2012) Assessment of CpTi surface properties after nitrogen ion implantation with various doses and energies. Metall Mater Trans A 43:4185–4193
53. Baboukani AR, Adelowo E, Agrawal R, Khakpour I, Drozd V, Li W, Wang C (2018) Electrostatic spray deposited Sn-SnO_2-CNF composite anodes for lithium ion storage. ECS Trans 85:331–336
54. Manoli K, Nakhla G, Feng M, Sharma VK, Ray AK (2017) Silica gel-enhanced oxidation of caffeine by ferrate(VI). Chem Eng J 330:987–994
55. Foroughi P, Rabiei Baboukani A, Franco Hernandez A, Wang C, Cheng Z (2018) Phase control during synthesis of nanocrystalline ultrahigh temperature tantalum-hafnium diboride powders. J Am Ceram Soc 101:5745–5755
56. Zolfaghari S, Baboukani AR, Ashrafi A, Saatchi A (2018) Investigation the effects of Na_2MoO_4 as an inhibitor on electrochemical corrosion behavior of 316L stainless steel in LiBr solution. Zaštita Materijala 59:108–116
57. Saberi F, Boroujeny BS, Doostmohamdi A, Baboukani AR, Asadikiya M (2018) Electrophoretic deposition kinetics and properties of ZrO_2 nano coatings. Mater Chem Phys 213:444–454
58. Saito G, Hosokai S, Akiyama T (2011) Synthesis of ZnO nanoflowers by solution plasma. Mater Chem Phys 130:79–83
59. Sharma VK, Tolan S, Bumbálek V, Macova Z, Bouzek K (2016) Stability of ferrate(VI) in 14 M NaOH–KOH mixtures at different temperatures. ACS Symp Ser 1238:241–253
60. Sun X, Zhang Q, Liang H, Ying L, Xiangxu M, Sharma VK (2016) Ferrate(VI) as a greener oxidant: electrochemical generation and treatment of phenol. J Hazard Mater 319:130–136
61. Tan W-F, Yu Y-T, Wang M-X, Liu F, Koopal LK (2014) Shape evolution synthesis of monodisperse spherical, ellipsoidal, and elongated hematite (α-Fe_2O_3) nanoparticles using ascorbic acid. Cryst Growth Des 14(157):164

62. Wu W, Wu Z, Yu T, Jiang C, Kim WS (2015) Recent progress on magnetic iron oxide nanoparticles: synthesis, surface functional strategies and biomedical applications. Sci Technol Adv Mater 16:023501
63. El Maghraoui A, Zerouale A, Ijjaali M, Sajieddine M (2013) Synthesis and characterization of ferrate(VI) alkali metal by electrochemical method. Adv Mater Phys Chem 3:83–87
64. Lescuras-Darrou V, Lapicque F, Valentin G (2002) Electrochemical ferrate generation for waste water treatment using cast irons with high silicon contents. J Appl Electrochem 32:57–63